NIH Public Access
Author Manuscript
Phys Med Biol. Author manuscript; available in PMC 2011 February 7.

Published in final edited form as:
Phys Med Biol. 2011 February 7; 56(3): 721–733. doi:10.1088/0031-9155/56/3/012.

Renal uptake of bismuth-213 and its contribution to kidney radiation dose following administration of actinium-225-labeled antibody

J Schwartz[1,5], **J S Jaggi**[2], **J A O'Donoghue**[1], **S Ruan**[3], **M McDevitt**[4], **S M Larson**[3], **D A Scheinberg**[4], and **J L Humm**[1]

[1] Department of Medical Physics, Memorial Sloan-Kettering Cancer Center, 1275 York Avenue, New York, NY 10065, USA

[2] Bristol-Myers Squibb, Plainsboro, NJ, USA

[3] Nuclear Medicine Service Department of Radiology, Memorial Sloan-Kettering Cancer Center, 1275 York Avenue, New York, NY 10065, USA

[4] Molecular Pharmacology and Chemistry, Sloan-Kettering Institute, 1275 York Avenue, New York, NY 10065, USA

Abstract

Clinical therapeutic studies using ^{225}Ac-labeled antibodies have begun. Of major concern is renal toxicity that may result from the three alpha-emitting progeny generated following the decay of ^{225}Ac. The purpose of this study was to determine the amount of ^{225}Ac and non-equilibrium progeny in the mouse kidney after the injection of ^{225}Ac-huM195 antibody and examine the dosimetric consequences. Groups of mice were sacrificed at 24, 96 and 144 h after injection with ^{225}Ac-huM195 antibody and kidneys excised. One kidney was used for gamma ray spectroscopic measurements by a high-purity germanium (HPGe) detector. The second kidney was used to generate frozen tissue sections which were examined by digital autoradiography (DAR). Two measurements were performed on each kidney specimen: (1) immediately post-resection and (2) after sufficient time for any non-equilibrium excess ^{213}Bi to decay completely. Comparison of these measurements enabled estimation of the amount of excess ^{213}Bi reaching the kidney (γ-ray spectroscopy) and its sub-regional distribution (DAR). The average absorbed dose to whole kidney, determined by spectroscopy, was 0.77 (SD 0.21) Gy kBq^{-1}, of which 0.46 (SD 0.16) Gy kBq^{-1} (i.e. 60%) was due to non-equilibrium excess ^{213}Bi. The relative contributions to renal cortex and medulla were determined by DAR. The estimated dose to the cortex from non-equilibrium excess ^{213}Bi (0.31 (SD 0.11) Gy kBq^{-1}) represented ~46% of the total. For the medulla the dose contribution from excess ^{213}Bi (0.81 (SD 0.28) Gy kBq^{-1}) was ~80% of the total. Based on these estimates, for human patients we project a kidney-absorbed dose of 0.28 Gy MBq^{-1} following administration of ^{225}Ac-huM195 with non-equilibrium excess ^{213}Bi responsible for approximately 60% of the total. Methods to reduce renal accumulation of radioactive progeny appear to be necessary for the success of ^{225}Ac radioimmunotherapy.

1. Introduction

Most radioimmunotherapy (RIT) clinical trials involve the use of antibodies labeled with β-emitting radionuclides (Kaminski *et al* 2005, Gopal *et al* 2003, Divgi *et al* 2004, Witzig *et al*

[5]Author to whom any correspondence should be addressed. schwarj1@mskcc.org.

NIH-PA Author Manuscript
NIH-PA Author Manuscript
NIH-PA Author Manuscript

NIH-PA Author Manuscript

NIH-PA Author Manuscript

NIH-PA Author Manuscript

2002, Bander *et al* 2005). Advantages of β-emitters include their relatively long range (e.g. the average range of ^{90}Y β-emission is 3.9 mm in soft tissue); as a result, the radiolabeled antibody need not localize in or on every cancer cell to be effective since substantial radiation dose may be delivered by cross-fire. Other advantages of β-emitters include availability at low cost, convenience and widespread clinical experience in their handling.

There is, however, growing interest in the development of therapies using antibodies labeled with α-particle-emitting radionuclides (Miederer *et al* 2008, Sgouros 2008, Boskovitz *et al* 2009, Song *et al* 2009, Milenic *et al* 2010, McDevitt *et al* 2001). Alpha particles have a relatively short range in tissue (<90 μm) and a high linear energy transfer (LET), depositing large amounts of energy per unit track length. The ratio of energy deposited by an α-particle traversal of a small volume, such as a cell nucleus, to that deposited by a β-particle is typically ~400. Moreover, the biological impact per unit dose is further enhanced by a factor of at least 3 due to the higher relative biological effectiveness (RBE) of α- versus β-radiation for the endpoint of cellular reproductive failure (Adelstein *et al* 2002). The net result of these factors is that the α-particle dose corresponding to D_0 (the radiation dose required to reduce surviving fraction by a factor e^{-1}) is reached with only 2 or 3 hits per cell, compared to more than 1000 hits for low LET radiations (Humm 1986). Finally, the shorter range of α-particles will result in less radiation cross-fire to normal tissues.

Until recently, α-particle RIT has focused on radionuclides that emit single α-particles, such as ^{211}At (Akabani *et al* 2006, Zalutsky *et al* 2008) and ^{213}Bi (Jurcic *et al* 2002, Friesen *et al* 2007). While these studies demonstrated aspects of feasibility and safety of α-particle-based therapies, efficacy was typically limited by the short half-lives of ^{211}At and ^{213}Bi (7.2 h and 46 min respectively). Short-lived radionuclides are pharmacokinetically incompatible with antibody-targeted therapy due to the significant time required (typically >1 day) to achieve a targeting differential, during which the vast majority of activity will decay.

Recently, interest has focused on ^{225}Ac as a potential α-emitting radionuclide for RIT (Miederer *et al* 2008, Song *et al* 2009). ^{225}Ac has a ten day half-life, long enough to allow differential tumor accumulation and possibly cellular internalization of radiolabeled antibody prior to decay. In addition, the total decay of ^{225}Ac, from original parent through successive progeny, involves the emission of four α-particles. Thus, the decay of ^{225}Ac at a tumor site, especially if the construct were internalized, could result in an extremely radiotoxic event.

Figure 1 summarizes the decay scheme of ^{225}Ac. The first decay results in a ^{221}Fr nucleus with a recoil kinetic energy (mean 120 keV) significantly greater than the chemical bond energies of any chelating agent. The fate of ^{221}Fr and its downstream progeny will thus depend upon the ^{225}Ac decay site. If ^{225}Ac decays within tumor, especially if internalized, some or all of the subsequent decays may also occur in tumor. Other scenarios (e.g. ^{225}Ac decay in the circulation) could result in some or all subsequent decays occurring elsewhere.

In terms of non-invasive imaging, there are two detectable events: (1) a 218 keV gamma-ray emitted with the α-decay of ^{221}Fr to ^{217}At and (2) a 440 keV gamma-ray emitted with the β-decay of ^{213}Bi to ^{213}Po. The latter of these has been successfully imaged in clinical studies (Sgouros *et al* 1999). Due to its short half-life (32 msec), it can reasonably be assumed that the decay of ^{217}At occurs at the same location as that of ^{221}Fr. However, the half-life of ^{213}Bi is sufficiently long (46 min) for significant translocation to occur prior to its decay. By imaging separately the 218 keV and 440 keV photons, it may be possible to determine the spatial locations of ^{221}Fr and ^{213}Bi atoms. Thus, for non-invasive imaging the best estimate of the location of ^{225}Ac would have to be derived from that of ^{221}Fr. In pre-clinical

UH & EURATOM Ex. 2019-002
Fusion v. Universität Heidelberg, et al.
IPR2023-00551

NIH-PA Author Manuscript

NIH-PA Author Manuscript

NIH-PA Author Manuscript

systems, this situation may be improved by the use of invasive methods that enable the location of ^{225}Ac to be determined.

Previous biodistribution studies with ^{225}Ac-huM195 antibody in mice (Jaggi *et al* 2005) and non-human primates (Miederer *et al* 2004) have shown accumulation of ^{213}Bi in kidney suggesting this may be dose limiting for ^{225}Ac-antibody therapy. Early studies on the metabolism of bismuth compounds suggested preferential uptake in the renal cortex (Russ *et al* 1975, Slikkerveer and Dewolff 1989, Szymanska *et al* 1977). Speidel *et al* (1991) showed that while bismuth isotopes were excreted through the kidney, there was non-negligible (3–5%) longer term retention. Furthermore, the kidney is particularly sensitive to radiation damage (Emami *et al* 1991, O'Donoghue 2004). The focus of this study was to use invasive methods to quantify the contributions to absorbed radiation dose in kidney from ^{225}Ac arriving as radiolabeled intact antibody versus ^{213}Bi arriving in the form of a dissociated radiometal following ^{225}Ac decay elsewhere in the body. Our long-term goal is to better understand kidney dosimetry for ^{225}Ac-labeled antibody therapies.

2. Methods

Experiments were performed using 4–12 week old female BALB/C mice obtained from Taconic (Germantown, NY). All animal studies were conducted according to the NIH Guide for the Care and Use of Laboratory Animals and were approved by the Institutional Animal Care and Use Committee at Memorial Sloan-Kettering Cancer Center.

A total of 12 anesthetized mice were each injected with ^{225}Ac-huM195 (22.2 kBq in 100 μl) in the retro-orbital venous plexus. Animals in groups of 4 were sacrificed at 24, 96 and 144 h post-administration. Immediately following sacrifice, both kidneys were removed from each animal. One kidney was used for nuclear spectroscopy measurements with a HPGe detector. The other was rapidly frozen and sectioned for histology and DAR.

2.1. Labeling huM195 with ^{225}Ac

Actinium-225 was provided by Oak Ridge National Laboratory (Oak Ridge, TN). The humanized anti-CD33 antibody (IgG1) huM195 antibody (Protein Design Labs) was labeled with ^{225}Ac using a two-step labeling method, as described previously (McDevitt *et al* 2002). Radiochemical purity was 95–99% by instant thin-layer chromatography. The specific activity of ^{225}Ac-huM195 was approximately 3.2 MBq mg^{-1}.

2.2. Nuclear spectroscopy

Immediately after sacrifice, one kidney was placed in a vial and positioned 10 cm from the front face of a Princeton Gamma Tech PGT IGC P-Type HPGe (Princeton, NJ 08540) detector connected to a Canberra Industries multi-channel analyzer system (Meriden, CT) and counted for 30 min. The system energy resolution (FWHM) was 1.8 keV for 1336 keV γ-rays. The digitized signal was stored as an energy histogram and total counts in the spectral peaks (i.e. area under the curve) corresponding to 218 keV (^{221}Fr) and 440 keV photons (^{213}Bi) were determined. Thereafter, kidneys were stored in a refrigerator for at least 24 h and the measurements repeated. The second measurement reflected only activity that was originally present in the sample as ^{225}Ac. The system calibration factor was estimated by measuring a ^{225}Ac standard of known activity in equilibrium with its progeny, positioned at the same location as the kidney samples.

2.3. Autoradiography and tissue histology

The second kidney from each mouse was embedded in OCT (Optimum Cutting Tissue, Miles Inc., Elkhart, IN) and frozen on dry ice in a cryo-mold. Sets of ten contiguous 8 μm

UH & EURATOM Ex. 2019-003
Fusion v. Universität Heidelberg, et al.
IPR2023-00551

NIH-PA Author Manuscript

NIH-PA Author Manuscript

NIH-PA Author Manuscript

thick tissue sections were cut using a Microm HM500 cryostat microtome (Microm International, Walldorf, Germany) and deposited onto poly-L-lysine coated glass microscope slides. Alternate sections were used for DAR and histological staining. Activity standards were constructed by mixing known activities of ^{225}Ac in known volumes of OCT compound, pouring into cryo-molds and freezing on dry ice. Thereafter, sections of 8 μm thickness were cut and collected on glass microscope slides in a manner identical to that used for the kidney specimens.

Digital autoradiograms were obtained of the tissue sections and two ^{225}Ac standards, all of which were covered with a thin Mylar film and placed in a film cassette against a Fuji film BAS-MS2325 imaging plate (Fuji Photo Film Co, Tokyo, Japan). Two exposures were made: (1) a 1 h exposure begun 45–60 min after sacrifice and (2) a 24 h exposure begun at least 24 h post-sacrifice. As for the case of nuclear spectroscopy, the second DAR measurement reflected only activity originally present in the sample as ^{225}Ac.

Exposed phosphor plates were read by a Fujifilm BAS-1800II bio-imaging analyzer (Fuji Photo Film Co, Tokyo, Japan) generating digital images with 50 μm pixel dimensions. DAR image intensity, expressed in the machine readout parameter of photo-stimulated luminescence per square mm (PSL mm^{-2}), was quantified using Multi Gauge software (version 2.2, Fujifilm, Tokyo, Japan). To minimize differences associated with variable plate sensitivity, a single phosphor plate was used for all sample exposures.

Tissue sections for histology were fixed in 10% phosphate-buffered formalin for 5 min, washed twice, air dried and stained with hematoxylin and eosin. Digital images (pixel dimension 12 μm) were obtained with an Olympus BX60 System Microscope (Olympus America Inc, Melville, NY) equipped with a motorized stage (Prior Scientific Inc, Rockland, MA). Subsequently, the H & E images were re-sampled to the same resolution as that of the DAR data. Ten DAR images (early and late exposures of five tissue sections) were manually aligned to the histologic images using rigid planar transforms, consisting of translations and rotations only. Once aligned, the five DAR images for each exposure time were averaged to create a single mean-intensity DAR image. For each kidney, two DAR images corresponding to early and late exposures were thus obtained. Regions of interest (ROI) corresponding to the cortical and medullary regions of each kidney were manually drawn on each histologic image and then overlaid onto the corresponding aligned DAR image. The mean PSL mm^{-2} in each ROI was then recorded. ROIs were also drawn on the co-exposed ^{225}Ac standards.

3. Data analysis

The analysis was based on the following rationale and assumptions.

- Measurements performed more than 24 h after sacrifice (late measurements) are due entirely to activity that was originally present in the sample as ^{225}Ac and reflect the decay of ^{225}Ac and its progeny in equilibrium.
- Measurements performed immediately after sacrifice (early measurements) may contain a contribution from non-equilibrium excess ^{213}Bi. No attempt was made to quantify non-equilibrium excess ^{221}Fr due to its short half-life.
- ^{225}Ac in the kidney and progeny produced from ^{225}Ac that decayed the kidney are in equilibrium, that is, any non-equilibrium excess ^{213}Bi is due to material that arrived in the kidney in the form of dissociated ^{213}Bi.

The contribution of any radioactive species to a measurement is proportional to the total number of decays of the species that occurs over the time of measurement. If a measurement

UH & EURATOM Ex. 2019-004
Fusion v. Universität Heidelberg, et al.
IPR2023-00551

NIH-PA Author Manuscript

NIH-PA Author Manuscript

NIH-PA Author Manuscript

of duration, δ, begins at a time, τ, after sacrifice, then the total number of decays during measurement, $\tilde{A}$, is given by

$$\tilde{A} = \int_{\tau}^{\tau+\delta} A_{\text{sac}} \mathrm{e}^{-\lambda t} \mathrm{d}t \tag{1}$$

where A_{sac} is the activity in the sample at the time of sacrifice and λ is the appropriate decay constant (= $\ln(2)/T_{1/2}$), i.e.

$$\tilde{A} = \frac{A_{\text{sac}}}{\lambda} \mathrm{e}^{-\lambda\tau}(1 - \mathrm{e}^{-\lambda\delta}). \tag{2}$$

For ^{225}Ac and its progeny in equilibrium, the appropriate decay constant is that of ^{225}Ac as the activities of all equilibrium progeny are equal to that of ^{225}Ac. For non-equilibrium ^{213}Bi, the appropriate decay constant is that of ^{213}Bi.

The total number of decays is related to the measured value, N, by

$$\tilde{A} = \kappa N \tag{3}$$

where κ is a calibration factor, estimated using standards of known activity.

The activity at the time of sacrifice can therefore be calculated from N by

$$A_{\text{sac}} = \kappa \lambda N \frac{\mathrm{e}^{\lambda\tau}}{(1 - \mathrm{e}^{-\lambda\delta})}. \tag{4}$$

3.1. Nuclear spectroscopy

The activity of ^{225}Ac and its progeny in equilibrium at the time of sacrifice was estimated based on the late measurement using equation (4). For the late measurement the ratio of the 218 (^{221}Fr) to 440 keV (^{213}Bi) spectral peak counts was equal to that of the ^{225}Ac standard. Independent estimates of A_{sac} were made for each of the 218 keV and 440 keV spectral peaks. These were used to generate expected values for the number of counts in the 440 keV peak at the early measurement due to ^{225}Ac and progeny in equilibrium. The differences between the expected values and the actual measured values (ΔN) represented the contribution of non-equilibrium, excess ^{213}Bi at the time of measurement. Equation (4) was then used with N replaced by ΔN to derive estimates of non-equilibrium (i.e. excess) ^{213}Bi activity at the time of sacrifice.

3.2. Autoradiography

The metric used for DAR analysis was mean PSL mm^{-2} value for each ROI. Values of A_{sac} per unit volume for ^{225}Ac and progeny in equilibrium were estimated from the late DAR using equation (4) and calibration factors (in units of Bq s ml^{-1} per PSL mm^{-2}) derived from the activity standards. The calculated A_{sac} for ^{225}Ac were then used to generate expected values of PSL mm^{-2} for the early measurement. The differences between expected and actual values for the early measurements were taken to represent the contribution of

UH & EURATOM Ex. 2019-005
Fusion v. Universität Heidelberg, et al.
IPR2023-00551

NIH-PA Author Manuscript

NIH-PA Author Manuscript

NIH-PA Author Manuscript

non-equilibrium excess ^{213}Bi. Analysis of the output of the DAR data provided estimates of the relative contributions of ^{225}Ac (and equilibrium progeny) and non-equilibrium excess ^{213}Bi to the cortex and medulla, defined using co-registered H&E-stained tissue sections. The partitioning of the whole kidney dose, estimated by spectroscopy as described above, into separate cortex and medulla doses was performed using this relative uptake data.

3.3. Kidney dosimetry

The absorbed radiation dose to the kidney is determined by two principal components.

1. A component due to ^{225}Ac present in the kidney and its equilibrium progeny. The long effective half-life (~96 h) of ^{225}Ac-DOTA-huM195 antibody in mice (Jaggi *et al* 2005) is indicative of the *in vivo* stability of the construct and implies that most ^{225}Ac arrives in the kidney in the form of intact radio-antibody.
2. A component due to ^{213}Bi resulting from the decay of ^{225}Ac elsewhere in the body (primarily the circulation) that subsequently translocates to the kidney. Renal uptake of ^{213}Bi has been shown in previous studies (Newton *et al* 2001). As free ^{213}Bi is constantly being generated by the decay of ^{225}Ac, it is anticipated to have an apparent effective half-life equivalent to that of ^{225}Ac. The dosimetric contribution of non-equilibrium ^{213}Bi will thus be significantly greater than its short (46 min) physical half-life would otherwise suggest.

Using the methods described above, we separately estimated the two components of kidney-absorbed dose. The activity concentrations of equilibrium ^{225}Ac and non-equilibrium excess ^{213}Bi were evaluated at each sacrifice time to generate two activity concentration-time profiles. Cumulated activity concentrations, $\tilde{C}_x$, in the kidney for each radionuclide (x) were then derived by fitting mono-exponential functions to the activity concentration-time data and integrating to infinity. The absorbed dose to the kidney for radionuclide (x), D_x, was then given by

$$D_x = \tilde{C}_x \Delta_x \tag{5}$$

where Δ_x is the absorbed dose constant for the non-penetrating α and β emissions of ^{225}Ac and progeny (4.40×10^{-12} J) or ^{213}Bi (1.33×10^{-12} J) as appropriate. The penetrating photon emissions which contribute <1% of the total radiation dose were ignored.

3.4. Dosimetric projections for human patients

In order to derive a projected estimate of human kidney-absorbed dose it was assumed that the fractional uptake of administered activity in kidney (A_k/A_0) adjusted for relative fractional organ mass is the same in mice and humans. Specifically,

$$\frac{A_{\mathrm{k(human)}}}{A_{0\mathrm{(human)}}} = \frac{A_{\mathrm{k(mouse)}}}{A_{0\mathrm{(mouse)}}} \frac{m_{k\mathrm{(human)}}}{m_{\mathrm{WB(human)}}} \frac{m_{\mathrm{WB(mouse)}}}{m_{k\mathrm{(mouse)}}} \tag{6}$$

where A_0 and A_k denote administered activity and activity in kidney respectively. Standard values of whole body and kidney masses for human (Stabin *et al* 2005) and mouse (Stabin *et al* 2006) were used.

In terms of cumulated activity concentration (i.e. per unit mass) in kidney, $\tilde{C}_x$, the relationship reduces to

UH & EURATOM Ex. 2019-006
Fusion v. Universität Heidelberg, et al.
IPR2023-00551

NIH-PA Author Manuscript

NIH-PA Author Manuscript

NIH-PA Author Manuscript

$$\tilde{C}_{x(\text{human})}=\tilde{C}_{x(\text{mouse})}\frac{A_{0(\text{human})}}{A_{0(\text{mouse})}}\frac{m_{\text{WB(mouse)}}}{m_{\text{WB(human)}}}. \quad (7)$$

Projected absorbed doses were then calculated using equation (5).

4. Results

4.1. Nuclear spectroscopy

Figure 2 shows representative early and late γ-ray spectra for kidneys removed at 24, 96 and 144 h after injection of ^{225}Ac-huM195. It is apparent that the heights of the peaks of interest (218 keV and 440 keV) are dependent on the time of sacrifice and that the ratios of these heights are dependent on the time of measurement. The average count ratios (440/218) for all excised kidneys were 4.8 (SD 0.6) and 1.2 (SD 0.1) for early and late measurements respectively, with no apparent dependence on the time of sacrifice. Figure 3 plots the mean (±SD) values of the activity concentrations of ^{225}Ac and ^{213}Bi in kidney at the times of sacrifice together with the best-fitting mono-exponential clearance curves. These results are consistent with the continual replenishment of ^{213}Bi in the kidney by new atoms generated by ^{225}Ac decays in the rest of body, leading to an effective half-life (4.6 day) similar to that of ^{225}Ac (6.7 day). The results also indicate that the majority of activity in the kidneys at the time of sacrifice was in the form of non-equilibrium ^{213}Bi.

4.2. Autoradiography and histology

Figure 4 shows a set of images (H&E stained section with early and late DAR) of three kidneys removed at 24, 96 and 144 h after injection of ^{225}Ac-huM195 illustrating the placement of cortical and medullary ROI on the H&E sections and their transfer to the DAR. In qualitative terms, it is apparent that the late DAR show enhanced cortical uptake, whereas the early DAR show similar uptake in both cortex and medulla. This was a universal finding for all kidney samples examined and indicates that ^{225}Ac was primarily present in the renal cortex, probably in the form of antibody conjugate. In contrast, non-equilibrium-free ^{213}Bi was more likely to be present in the renal medulla.

Using the previously described methods, the average cortex:medulla ratios for all excised kidneys were 1.9 (SD 0.2) and 0.4 (SD 0.3) for equilibrium ^{225}Ac and non-equilibrium ^{213}Bi respectively. Consistent with the nuclear spectroscopy results there was no systematic dependence of these ratios on the time of sacrifice. These results indicate that, of the ^{225}Ac-huM195 present in the kidneys, the concentration was approximately two times greater in the cortex than in the medulla; whereas activity arriving in the form of ^{213}Bi was preferentially located in the renal medulla at a concentration approximately two times greater than in the cortex.

4.3. Kidney dosimetry

The spectroscopic data enabled estimation of the average absorbed radiation dose from the combination of equilibrium ^{225}Ac and non-equilibrium ^{213}Bi to the entire kidney. Based on this analysis, the estimated absorbed dose delivered to the mouse kidney by the administration of 22.2kBq of ^{225}Ac-huM195 was 17.4 (SD 4.8) Gy (i.e. 0.78 Gy kBq^{-1}). Of this total, the contribution due to activity arriving in the kidney in the form of ^{213}Bi was estimated to be 10.4 (SD 3.7) Gy. Incorporation of the differing relative concentrations of ^{225}Ac and ^{213}Bi in cortex and medulla derived from DAR analysis led to differential absorbed dose estimates for the two renal components. Assuming relative volumes of 70% and 30% for cortex and medulla (including renal pelvis) as per MIRD pamphlet 19 (Bouchet

UH & EURATOM Ex. 2019-007
Fusion v. Universität Heidelberg, et al.
IPR2023-00551

NIH-PA Author Manuscript

NIH-PA Author Manuscript

NIH-PA Author Manuscript

et al 2003), the absorbed dose estimates were 15 (SD 4) Gy to the cortex and 23 (SD 7) Gy to the medulla. It is noteworthy that a large component (18.2 (SD 6) Gy) of the estimated absorbed dose to the renal medulla was delivered by non-equilibrium excess ^{213}Bi generated from extra-renal decays of ^{225}Ac. Dosimetry estimates for mouse kidney are summarized in table 1.

4.4. Dosimetric projections for human patients

The projected absorbed dose to kidney for human patients derived as described in methods was 0.28 Gy MBq^{-1} of which 0.11 Gy MBq^{-1} was due to activity arriving in the form of ^{225}Ac and 0.17 Gy MBq^{-1} to non-equilibrium excess ^{213}Bi. Human dosimetry projections are summarized in table 1. The separate projections for cortex and medulla were derived by proportionality with the dose estimates for mouse kidney.

5. Discussion

The main aim of this study was to differentially estimate the amount of ^{225}Ac-labeled antibody and non-equilibrium progeny in the kidney, likely to be the dose limiting normal tissue for ^{225}Ac RIT (Jaggi *et al* 2005). This was primarily achieved by γ-ray spectroscopy, with additional sub-regional information provided by DAR. The key features of the methodology were the ability to perform measurements very rapidly (within 10 min in the case of γ-ray spectroscopy) after animal sacrifice and repeat them on the same samples after any non-equilibrium excess had decayed. These requirements constrained the possible techniques that could be used. In particular, the consequential alteration or destruction of the biological specimen precluded techniques such as emulsion autoradiography or liquid scintillation counting. Although DAR is a suitable method it currently lacks the spatial resolution to identify uptake at a cellular or sub-cellular level and is, in that sense, sub-optimal. Comparison of γ-ray spectra at early and late times post-sacrifice enabled the amount of non-equilibrium excess ^{213}Bi to be estimated. It was shown that non-equilibrium ^{213}Bi (resulting from the extra-renal decay of ^{225}Ac) was a major contributor to kidney-absorbed dose and in the renal medulla was responsible for 80% of the total dose.

Mechanistically, our understanding is that the initial decay of ^{225}Ac dissociates the first progeny ^{221}Fr from the antibody-chelate. The blood plasma will contain a steady-state equilibrium mixture of (antibody-associated) ^{225}Ac and (non-antibody-associated) progeny. ^{213}Bi in blood plasma which may be bound to transferrin (Sun and Szeto 2003, Miquel *et al* 2004) is of particular significance because of its preferential kidney uptake, possibly mediated by bismuth-binding metallothioneins (Sun *et al* 1999, Garrett *et al* 1999). The level of non-equilibrium ^{213}Bi in the kidney is continuously replenished by the plasma steady state and is greater than the amount of ^{213}Bi produced by the *in situ* decay of ^{225}Ac in kidney. Our data show an almost constant ratio (approx 7:1) between ^{225}Ac (and by inference equilibrium ^{213}Bi) and non-equilibrium ^{213}Bi. These findings are highly significant for clinical applications of ^{225}Ac-labeled antibody therapy. In principle, ^{225}Ac is a good pharmacokinetic match with antibodies that require significant time to achieve a targeting differential. However, the downside is that such molecules remain present for a protracted time, primarily in the blood plasma, and, if labeled with ^{225}Ac, will be continuous generators of alpha-emitting progeny with essentially no tumor selectivity. Given the apparently high level of renal uptake of ^{213}Bi, the radiobiological potency of alpha particles and the clinical significance of renal toxicity, it will be essential to develop methods to reduce kidney accumulation of radioactive progeny. Possible approaches include inhibition of renal absorption or acceleration of renal (or other) clearance. Preliminary studies (Jaggi *et al* 2006) have explored the use of metal chelators (DMSA, DMPS and Ca-DTPA) to scavenge ^{213}Bi atoms and of non-radioactive Bi atoms to block the renal binding sites of ^{213}Bi. Renal uptake of ^{213}Bi was reduced by these interventions (14–45% by metal

UH & EURATOM Ex. 2019-008
Fusion v. Universität Heidelberg, et al.
IPR2023-00551

NIH-PA Author Manuscript

NIH-PA Author Manuscript

NIH-PA Author Manuscript

chelation; 11–16% by cold Bi). These authors also found that the use of diuretics (with or without metal chelation) further reduced ^{213}Bi accumulation in the kidney. Approaches such as these may improve sparing of this potentially dose limiting organ and will probably be mandatory for the successful clinical implementation of ^{225}Ac-antibody therapy.

We recently initiated a phase I clinical trial using ^{225}Ac-huM195 antibody at MSKCC. Although the initial administered activity (18.5 kBq kg^{-1}/0.5 μCi kg^{-1}) is insufficient to permit imaging, such studies are planned at higher administered activities. It will be of considerable interest to see if clinical non-invasive imaging is capable of accurately assessing the biodistribution of ^{225}Ac and its troublesome progeny.

6. Conclusions

In this study, we quantified in mice the renal uptake of non-equilibrium ^{213}Bi produced by ^{225}Ac decays in the rest of body and assessed its relative contribution to kidney-absorbed dose following administration of ^{225}Ac-labeled antibody. We found that non-equilibrium ^{213}Bi is responsible for a significant fraction of the total radiation dose to kidney. For the renal medulla, the dosimetric contribution of non-equilibrium ^{213}Bi was as high as 80%. The absorbed dose to the mouse kidney per kBq of administered ^{225}Ac-huM195 was estimated to be 0.77 Gy. For human patients we project a kidney-absorbed dose of 0.28 Gy MBq^{-1} following administration of ^{225}Ac-huM195 with non-equilibrium excess ^{213}Bi responsible for approximately 60% of this total. These findings reinforce the importance of developing methods to reduce renal accumulation of radioactive progeny in clinical applications of ^{225}Ac radioimmunotherapy.

References

Adelstein S, Green A, Howell R, Humm J, Leichner P, O'Donoghue J, Strand S, Wessels B. ICRU Report 67: absorbed-dose specification in nuclear medicine. J ICRU 2002;2

Akabani G, Carlin S, Welsh P, Zalutsky MR. *In vitro* cytotoxicity of At-211-labeled trastuzumab in human breast cancer cell lines: effect of specific activity and HER2 receptor heterogeneity on survival fraction. Nucl Med Biol 2006;33:333–47. [PubMed: 16631082]

Bander NH, Milowsky MI, Nanus DM, Kostakoglu L, Vallabhajosula S, Goldsmith SJ. Phase I trial of (177)lutetium-labeled J591, a monoclonal antibody to prostate-specific membrane antigen, in patients with androgen-independent prostate cancer. J Clin Oncol 2005;23:4591–601. [PubMed: 15837970]

Boskovitz A, McLendon RE, Okamura T, Sampson JH, Bigner DD, Zalutsky MR. Treatment of HER2-positive breast carcinomatous meningitis with intrathecal administration of alpha-particle-emitting At-211-labeled trastuzumab. Nucl Med Biol 2009;36:659–69. [PubMed: 19647172]

Bouchet LG, Bolch WE, Blanco HP, Wessels BW, Siegel JA, Rajon DA, Clairand I, Sgouros G. MIRD pamphlet no. 19: absorbed fractions and radionuclide S values for six age-dependent multiregion models of the kidney. J Nucl Med 2003;44:1113–47. [PubMed: 12843230]

Divgi CR, et al. Phase I clinical trial with fractionated radioimmunotherapy using I-13-labeled chimeric G250 in metastatic renal cancer. J Nucl Med 2004;45:1412–21. [PubMed: 15299069]

Emami B, Lyman J, Brown A, Coia L, Goitein M, Munzenrider JE, Shank B, Solin LJ, Wesson M. Tolerance of normal tissue to therapeutic irradiation. Int J Radiat Oncol Biol Phys 1991;21:109–22. [PubMed: 2032882]

Friesen C, Glatting G, Koop B, Schwarz K, Morgenstern A, Apostolidis C, Debatin KM, Reske SN. Breaking chemoresistance and radioresistance with [Bi-213]anti-CD45 antibodies in leukemia cells. Cancer Res 2007;67:1950–8. [PubMed: 17332322]

Garrett SH, Sens MA, Todd JH, Somji S, Sens DA. Expression of MT-3 protein in the human kidney. Toxicol Lett 1999;105:207–14. [PubMed: 10355541]

UH & EURATOM Ex. 2019-009
Fusion v. Universität Heidelberg, et al.
IPR2023-00551

NIH-PA Author Manuscript

NIH-PA Author Manuscript

NIH-PA Author Manuscript

Gopal AK, et al. High-dose radioimmunotherapy versus conventional high-dose therapy and autologous hematopoietic stem cell transplantation for relapsed follicular non-Hodgkin lymphoma: a multivariable cohort analysis. Blood 2003;102:2351–7. [PubMed: 12750161]

Humm JL. Dosimetric aspects of radiolabeled antibodies for tumor-therapy. J Nucl Med 1986;27:1490–7. [PubMed: 3528417]

Jaggi JS, Seshan SV, McDevitt MR, LaPerle K, Sgouros G, Scheinberg DA. Renal tubulointerstitial changes after internal irradiation with alpha-particle-emitting actinium daughters. J Am Soc Nephrol 2005;16:2677–89. [PubMed: 15987754]

Jaggi JS, Seshan SV, McDevitt MR, Sgouros G, Hyjek E, Scheinberg DA. Mitigation of radiation nephropathy after internal alpha-particle irradiation of kidneys. Int J Radiat Oncol Biol Phys 2006;64:1503–12. [PubMed: 16503385]

Jurcic JG, et al. Targeted at particle immunotherapy for myeloid leukemia. Blood 2002;100:1233–9. [PubMed: 12149203]

Kaminski MS, et al. I-131-tositumomab therapy as initial treatment for follicular lymphoma. N Engl J Med 2005;352:441–9. [PubMed: 15689582]

McDevitt MR, et al. Tumor therapy with targeted atomic nanogenerators. Science 2001;294:1537–40. [PubMed: 11711678]

McDevitt MR, Ma DS, Simon J, Frank RK, Scheinberg DA. Design and synthesis of Ac-225 radioimmunopharmaceuticals. Appl Radiat Isot 2002;57:841–7. [PubMed: 12406626]

Miederer M, McDevitt MR, Sgouros G, Kramer K, Cheung NKV, Scheinberg DA. Pharmacokinetics, dosimetry, and toxicity of the targetable atomic generator, Ac-225-HuM195, in nonhuman primates. J Nucl Med 2004;45:129–37. [PubMed: 14734685]

Miederer M, Scheinberg DA, McDevitt MR. Realizing the potential of the Actinium-225 radionuclide generator in targeted alpha particle therapy applications. Adv Drug Deliv Rev 2008;60:1371–82. [PubMed: 18514364]

Milenic DE, Brady ED, Garmestani K, Albert PS, Abdulla A, Brechbiel MW. Improved efficacy of alpha-particle-targeted radiation therapy. Cancer 2010;116:1059–66. [PubMed: 20127951]

Miquel G, Nekaa T, Kahn PH, Hémadi M, El Hage Chahine J-M. Mechanism of formation of the complex between transferrin and bismuth, and interaction with transferrin receptor 1. Biochemistry 2004;43:14722–31. [PubMed: 15544343]

Newton D, Talbot RJ, Priest ND. Human biokinetics of injected bismuth-207. Hum Exp Toxicol 2001;20:601–9. [PubMed: 11936573]

O'Donoghue J. Relevance of external beam dose-response relationships to kidney toxicity associated with radionuclide therapy. Cancer Biother Radiopharm 2004;19:378–87. [PubMed: 15285886]

Russ GA, Bigler RE, Tilbury RS, Woodard HQ, Laughlin JS. Metabolic studies with radiobismuth:1. Retention and biodistribution of Bi-206 in normal rat. Radiat Res 1975;63:443–54. [PubMed: 1162032]

Sgouros G. Alpha-particles for targeted therapy. Adv Drug Deliv Rev 2008;60:1402–6. [PubMed: 18541332]

Sgouros G, Ballangrud AM, Jurcic JG, McDevitt MR, Humm JL, Erdi YE, Mehta BM, Finn RD, Larson SM, Scheinberg DA. Pharmacokinetics and dosimetry of an alpha-particle emitter labeled antibody: Bi-213-HuM195 (anti-CD33) in patients with leukemia. J Nucl Med 1999;40:1935–46. [PubMed: 10565792]

Slikkerveer A, Dewolff FA. Pharmacokinetics and toxicity of Bismuth compounds. Med Toxicol Adv Drug Exp 1989;4:303–23.

Song H, Hobbs RF, Vajravelu R, Huso DL, Esaias C, Apostolidis C, Morgenstern A, Sgouros G. Radioimmunotherapy of breast cancer metastases with alpha-particle emitter Ac-225: comparing efficacy with Bi-213 and Y-90. Cancer Res 2009;69:8941–8. [PubMed: 19920193]

Speidel MT, Humm J, Bellerive MR, Mulkern R, Atcher RW, Hines JJ, Macklis RM. Assessment of dosimetry and early renal radiotoxicity after treatment with an alpha-particle emitting radiopharmaceutical. Antib Immunoconjug Radiopharm 1991;4:681–92.

Stabin MG, Peterson TE, Holburn GE, Emmons MA. Voxel-based mouse and rat models for internal dose calculations. J Nucl Med 2006;47:655–9. [PubMed: 16595500]

UH & EURATOM Ex. 2019-0010
Fusion v. Universität Heidelberg, et al.
IPR2023-00551

NIH-PA Author Manuscript

NIH-PA Author Manuscript

NIH-PA Author Manuscript

Stabin MG, Sparks RB, Crowe E. OLINDA/EXM: the second-generation personal computer software for internal dose assessment in nuclear medicine. J Nucl Med 2005;46:1023–7. [PubMed: 15937315]

Sun H, Li H, Harvey I, Sadler PJ. Interactions of bismuth complexes with metallothionein(II). J Biol Chem 1999;274:29094–101. [PubMed: 10506163]

Sun HZ, Szeto KY. Binding of bismuth to serum proteins: implication for targets of Bi(III) in blood plasma. J Inorg Biochem 2003;94:114–20. [PubMed: 12620681]

Szymanska JA, Mogilnicka EM, Kaszper BW. Binding of Bismuth in kidneys of rat—role of metallothionein-like proteins. Biochem Pharmacol 1977;26:257–8. [PubMed: 843396]

Witzig TE, et al. Randomized controlled trial of yttrium-90-labeled ibritumomab tiuxetan radioimmunotherapy versus rituximab immunotherapy for patients with relapsed or refractory low-grade, follicular, or transformed B-cell non-Hodgkin's lymphoma. J Clin Oncol 2002;20:2453–63. [PubMed: 12011122]

Zalutsky MR, Reardon DA, Akabani G, Coleman E, Friedman AH, Friedman HS, McLendon RE, Wong TZ, Bigner DD. Clinical experience with alpha-particle-emitting At-211: treatment of recurrent brain tumor patients with At-211-labeled chimeric antitenascin monoclonal antibody 81C6. J Nucl Med 2008;49:30–8. [PubMed: 18077533]

UH & EURATOM Ex. 2019-0011
Fusion v. Universität Heidelberg, et al.
IPR2023-00551

NIH-PA Author Manuscript

NIH-PA Author Manuscript

NIH-PA Author Manuscript

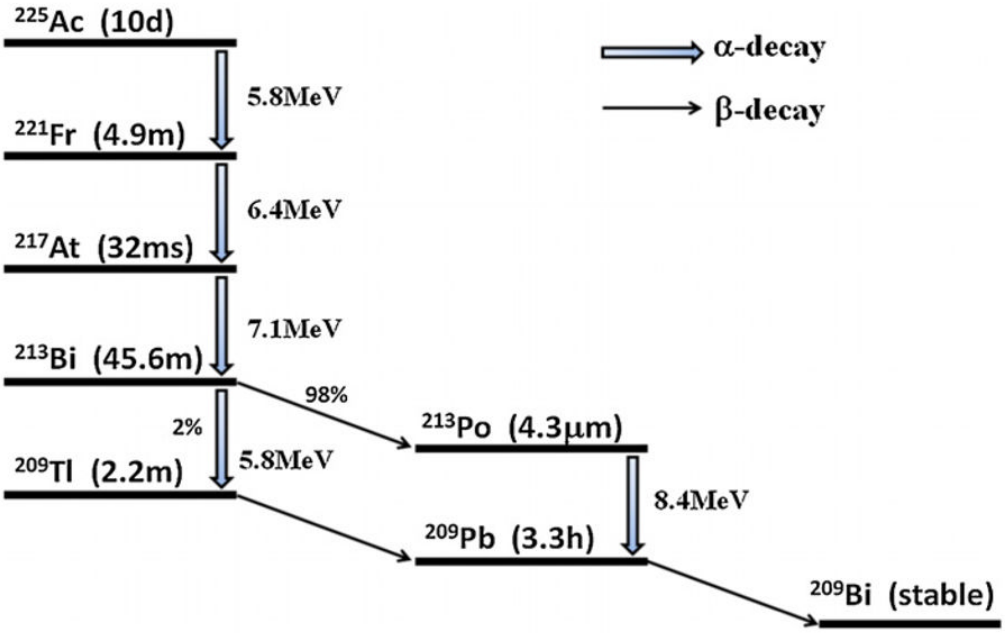

Figure 1.
^{225}Ac is part of the neptunium series decay chain eventually decaying to stable ^{209}Bi after the sequential emission of 4α-particles.

UH & EURATOM Ex. 2019-0012
Fusion v. Universität Heidelberg, et al.
IPR2023-00551

NIH-PA Author Manuscript

NIH-PA Author Manuscript

NIH-PA Author Manuscript

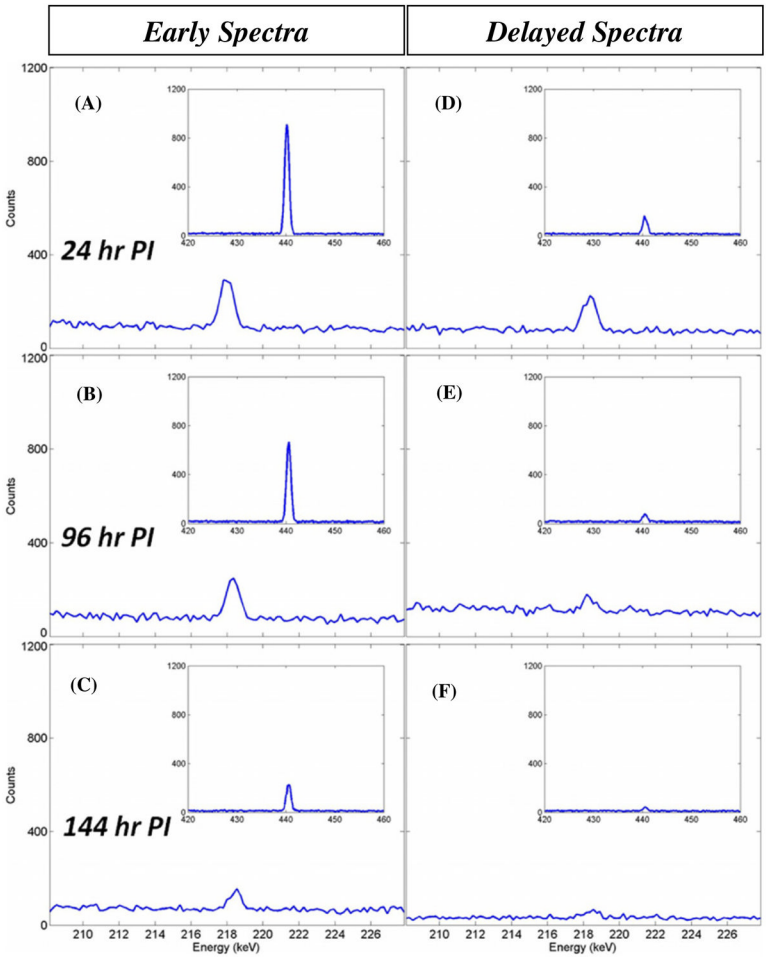

Figure 2.

Representative γ-ray spectra measured by HPGe detector: (A–C): early measurement for sacrifice times of 24, 96 and 144 h post-injection (PI). (D–F): measurements performed 24 h after sacrifice for each of the sacrifice times. The two peaks of interest shown are 218 keV (^{221}Fr) in the main window and 440 keV (^{213} Bi) in the inset.

UH & EURATOM Ex. 2019-0013
Fusion v. Universität Heidelberg, et al.
IPR2023-00551

NIH-PA Author Manuscript

NIH-PA Author Manuscript

NIH-PA Author Manuscript

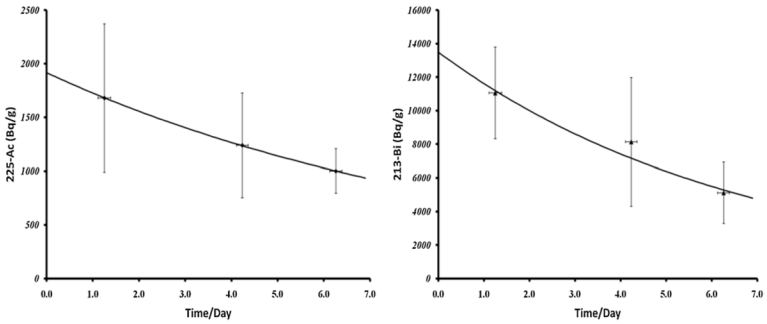

Figure 3.

Activity concentration-time relationships for ^{225}Ac and non-equilibrium excess ^{213}Bi in mouse kidney. Each point represents the mean of four measurements. The curves are monoexponential functions fitted to the data namely ^{225}Ac (Bq/g) = 1915 exp (−0.104 t): effective $T_{1/2}$ = 6.7 day ^{213}Bi (Bq/g) = 13490 exp (−0.150 t): effective $T_{1/2}$ = 4.6 day. Error bars denote standard deviations.

UH & EURATOM Ex. 2019-0014
Fusion v. Universität Heidelberg, et al.
IPR2023-00551

NIH-PA Author Manuscript

NIH-PA Author Manuscript

NIH-PA Author Manuscript

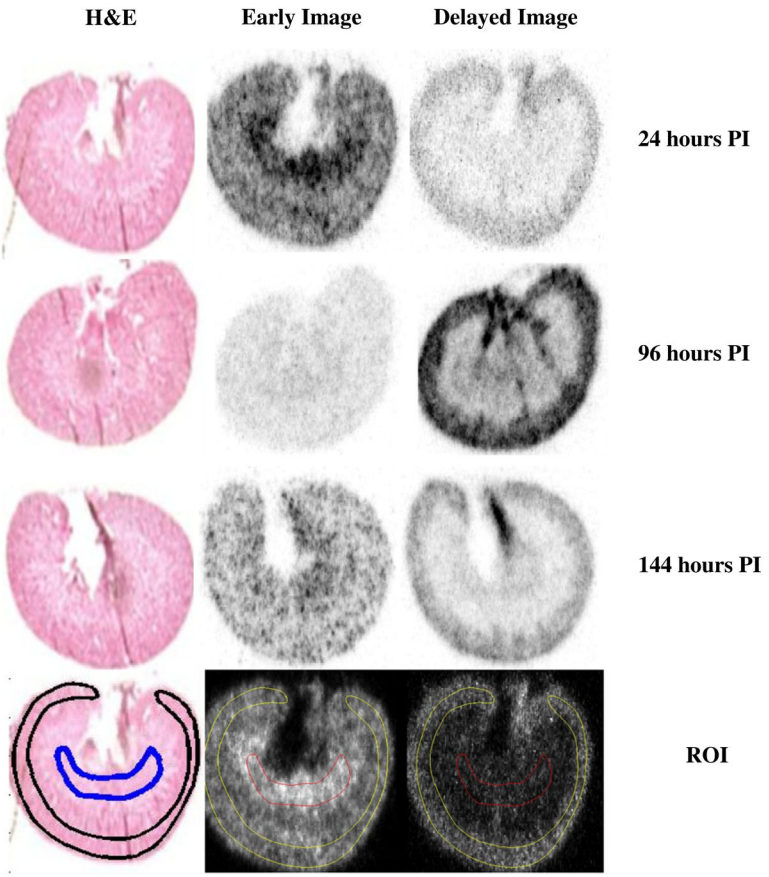

Figure 4.

Representative kidney images for each sacrifice time: H&E stained sections (left) and DAR from the same section exposed at early (middle) and late (right) times post-sacrifice. Bottom row: an example of ROI describing cortical and medullary regions of the kidney on an H&E-stained sections (left) that were transferred to aligned early (middle) and late (right) DAR images. All early (middle) images are shown with the same intensity scale, as are the late (right) images. The scale for the late images is 0.05× that of the early ones.

UH & EURATOM Ex. 2019-0015
Fusion v. Universität Heidelberg, et al.
IPR2023-00551

NIH-PA Author Manuscript NIH-PA Author Manuscript NIH-PA Author Manuscript

Table 1

Estimated radiation absorbed dose to mouse kidney and its sub-regions together with dosimetric projections for human kidney.

	Mouse (Gy kBq^{-1})			Human (Gy MBq^{-1})		
	^{225}Ac	^{213}Bi	Combined	^{225}Ac	^{213}Bi	Combined
Cortex	0.36 (0.16)	0.31 (0.11)	0.67 (0.20)	0.13	0.11	0.25
Medulla	0.19 (0.09)	0.81 (0.28)	1.0 (0.3)	0.07	0.30	0.37
Whole kidney	0.31 (0.14)	0.46 (0.16)	0.77 (0.21)	0.11	0.17	0.28

UH & EURATOM Ex. 2019-0016
Fusion v. Universität Heidelberg, et al.
IPR2023-00551